Hindawi Publishing Corporation
Journal of Biomedicine and Biotechnology
Volume 2011, Article ID 510827, 14 pages
doi:10.1155/2011/510827

Research Article

Loss of the NHE2 Na^+/H^+ Exchanger in Mice Results in Dilation of Folliculo-Stellate Cell Canaliculi

Marian L. Miller,[1] Anastasia Andringa,[1] Patrick J. Schultheis,[2] and Gary E. Shull[3]

[1] *Department of Environmental Health, University of Cincinnati, 3223 Eden Avenue, Cincinnati, OH 45267, USA*
[2] *Department of Biological Sciences, Northern Kentucky University, Nunn Drive, Highland Heights, KY 41099, USA*
[3] *Department of Molecular Genetics, Biochemistry and Microbiology, University of Cincinnati, 231 Albert Sabin Way, Cincinnati, OH 45267-0524, USA*

Correspondence should be addressed to Gary E. Shull, shullge@ucmail.uc.edu

Received 16 September 2010; Accepted 23 November 2010

Academic Editor: Monica Fedele

Genetic ablation of the NHE2 Na^+/H^+ exchanger causes gastric achlorhydria, absorptive defects in kidney and colon, and low fertility. Here we show that NHE2 is expressed in the pituitary, with the highest mRNA expression in pars distalis and lower expression in pars intermedia. In pars distalis of NHE2-null mice, prominent cyst-like dilatations of folliculo-stellate (FS) cell canaliculi developed with age, and there were increased FS cell area, accumulation of lipid in FS cell cytoplasm, redundancies in FS cell basement membrane, and other changes. The expansion of the canaliculi indicates that NHE2 is a major absorptive Na^+/H^+ exchanger in the luminal membranes lining the extensive network of channels formed by FS cells, which may provide a means of intrapituitary communication. The results suggest that NHE2 contributes to homeostatic regulation of the volume and composition of the canalicular fluid and may counter the secretory activity of the CFTR Cl^- channel, which is known to be expressed in pituitary.

1. Introduction

The pars distalis of the pituitary is composed of both granular and agranular cell types, the former largely hormone-producing cells [1], the latter forming a reticular and canalicular network in and around the granulated cells. Among the nongranulated cells are folliculo-stellate (FS) cells, which have numerous long cytoplasmic processes that insinuate among the endocrine cells. Neighboring FS cells are joined by well-developed junctional complexes forming an interconnected network of channels extending throughout the anterior pituitary, but particularly, the pars distalis [2, 3]. FS cells resemble polarized epithelial cells, with their apical surfaces containing microvilli and lining the lumen of the follicular cavities [2, 3]. Of relevance to the current study, there is evidence that FS cells play a role in the absorption of ions and water from the luminal spaces [4–6], which could involve the activity of an apical Na^+/H^+ exchanger.

Many aspects of metabolism, growth, stress, immunity, and reproduction are under the direct influence of granular cell secretions of the pars distalis [7]; however, the contribution of FS cells to intrapituitary communication and the mode(s) by which this occurs are less well understood. FS cells play a regulatory role both by secretion of paracrine factors, including activin, follistatin, and vascular endothelial growth factor [7, 8], and by intercellular communication via Ca^{2+} signals transmitted through gap junctions [9], which has been suggested to contribute to synchronization of hormone secretion by endocrine cells [9, 10]. A potential additional means of intrapituitary communication that could play a role in coordination of both FS cell and endocrine cell activities is the network of channels formed by the FS cells.

Previous studies showed that genetic ablation of the Na^+/H^+ exchanger isoform 2 (NHE2, gene symbol, *Slc9a2*), which is expressed at high levels in stomach [11], causes loss of gastric acid secretion, decreased viability of parietal cells,

and severe metaplasia and hyperplasia of the gastric mucosa [12, 13]. Histological abnormalities were not observed in the kidney or intestinal tract of NHE2-null (*Nhe2*$^{-/-}$) mice; however, they exhibited defects in the absorption of Na^+ and HCO_3^- in both the renal nephron and colonic crypts [14, 15], where NHE2 is also expressed, indicating that NHE2 can function as an absorptive Na^+/H^+ exchanger.

In the current study, it was shown that pituitaries from mice lacking NHE2 exhibited significant histopathological changes, particularly in the pars distalis and pars intermedia, both of which are derivatives of the primitive gut ectoderm. There was a greater accumulation of cytoplasmic lipid in FS cells and parenchymal cells, an undulating and reduplicated basement membrane, and decreased thickness of the pars intermedia, with a reduction of projections into the pars nervosa. However, the most striking change was a dilated FS cell canalicular system with large cyst-like spaces throughout the pars distalis, which is consistent with the loss of an absorptive ion transport mechanism in the luminal membrane of FS cells. Interestingly, the cystic fibrosis transmembrane conductance regulator (CFTR), a Cl^- channel that is defective in cystic fibrosis, is expressed in the pituitary gland [16] and likely mediates the cAMP-stimulated anion currents detected in cultured FS cells [4, 5]. A recent study showed that treatment with forskolin, which stimulates CFTR-mediated Cl^- secretion, affects secretion of growth hormone from pituitary slices in culture and suggested that loss of CFTR activity in the pituitary might be responsible, in part, for the reduced growth rates in both humans and pigs with cystic fibrosis [16]. The current results support the view [4] that FS cells play a major role in regulating the ionic composition and volume of the interstitial and follicular fluid and suggest that NHE2 serves as an absorptive Na^+/H^+ exchanger on the luminal surface of FS cells that counters fluid accumulation resulting from CFTR-mediated secretion of anions.

2. Materials and Methods

2.1. Animals. *Nhe2*$^{-/-}$ and age- and gender-matched wild-type (WT) mice of the original 129/SVJ and Black Swiss background [12] were used for these studies. All mice were housed in humidity and temperature controlled rooms, on a 12-hour light/dark cycle, with access to standard mouse chow and water ad libitum. Mice varied in age from 17 days to over 1 year old at euthanasia, with approximately equal numbers of males and females. Animals were separated into two age groups, age 1 : 17 days to 2.5 months, age 2 : 4 months–1 yr, and 37 mice were used. The number (n) of mice in any given analysis or bar graph is given in the legend. Animal protocols were approved by the University of Cincinnati Institutional Animal Care and Use Committee, and animal handlers were trained in an American Association of Assessment and Accreditation of Laboratory Animal Care facility.

2.2. Genotype Analysis. Genotypes were determined by PCR analysis of DNA isolated from tail biopsies using a set of 3 primers that simultaneously amplified wild-type and NHE2-null alleles [17]. Forward (5′-CATCTCTATCAC-AAGTTGCCCACAATCGTG-3′) and reverse (5′-GTGACT-GCATCGTTGAGCAGAGACTCG-3′) primers from the 5′ and 3′ ends of exon 2 amplified a 450-base pair product from the wild-type allele. A reverse primer (5′-GACAATAGC-AGGCATGCTGG-3′) complementary to sequences within the neomycin resistance gene cassette, which was inserted into exon 2 [12], and the forward primer described above amplified a 221-base pair product from the targeted allele.

2.3. Northern Blot and In Situ Hybridization Analyses. Northern blot analysis was performed as described by Schultheis et al. [12] using total RNA from colon and pooled pituitaries of 3-4 month-old mice and a 3.1 kb rat NHE2 cDNA probe spanning nucleotides 449–3561 (accession number L11236). *In situ* hybridization was performed as described by Simmons et al. [18] using ^{35}S-labeled antisense (AS) and sense (S) probes corresponding to codons 684–813 and detected using autoradiographic emulsion.

2.4. Tissue Processing. Pituitaries were removed immediately after euthanasia and immersed in 2% paraformaldehyde/2.5% glutaraldehyde or 4% paraformaldehyde in phosphate-buffered saline (PBS) for at least 24 hrs. Tissues were postfixed in 1% osmium tetroxide in either Millonig's buffer or PBS for 2 hrs, dehydrated stepwise in increasing concentrations of ethanol, with two changes of propylene oxide and one change each of 1 : 1 and 1 : 3 propylene oxide : Spurr (Electron Microscopy Sciences, Hatfield, PA). Tissues were left overnight in fresh 100% resin and flat-embedded in cut-off Beem capsules (Electron Microscopy Sciences, Hatfield, PA) the following day in fresh resin. Pituitaries were oriented in blocks to be cut transversely or coronally. Sections, 1.5 μm thick, were stained with toluidine blue for light microscopy. Pituitaries were also preserved in 4% paraformaldehyde, dehydrated in ethanol and xylene, blocked in paraffin, and serially sectioned at 5 μm. Some of these slides were stained with hematoxylin and eosin (H&E) and others were prepared for *in situ* hybridization. Pituitaries fixed for fine structural detail and opportunely oriented were thin-sectioned and stained with uranyl acetate and lead citrate for transmission electron microscopy.

2.5. Microscopy and Morphometry. Light microscopic morphology and morphometry were conducted on H&E stained sections as well as on plastic sections stained with toluidine blue. The Vd (percentage) of cytoplasmic elements was calculated from the number of intersections of a 320 point grid lying over any element/(320 minus the points over nontissue elements) $\times$ 100. The 320-point grid was printed directly onto digital light micrographs acquired from toluidine blue stained sections at a magnification of 100x. Micrographs were examined without prior knowledge of genotype. Intersections of that grid lying over the following cytoplasmic and nuclear features were counted for pars distalis: (1) FS cell canalicular space, (2) obvious FS cell cytoplasm and nuclei (mainly where the cells were

adjacent to canalicular lumens), (3) nuclei and cytoplasm of somatotrophs and mammotrophs (as a single group of cells containing large granules) and other endocrine cells (those with smaller granules), (4) lipid droplet inclusions, (5) blood vessels and vascular luminal contents (endothelium, red cells, and vascular space), and (6) negative areas (those which were not tissue content, such as grid bars, edges, folds, and tears). The number of cells per light micrograph was approximately 200; metaphase cells were counted and the percentage of cells in mitosis calculated. Although it was not possible to absolutely identify the cell types in 1.5 μm thick sections at the light microscopic level, morphological consistencies among cell types allowed for a reasonable separation of the large granule cells, granule cells with smaller granules, FS cells, and capillaries. FS cells are somewhat underrepresented in light micrographs because the thinness is just at the limits of the light microscope.

Basement membrane redundancy was quantified by drawing a line perpendicular to the endothelial cell basal lamina up through the basement membranes to the closest FS cell basal lamina. The mean number of basement membranes which intersected this line was calculated. Measurements of the thickness of the pars intermedia were obtained similarly, using both paraffin and plastic sections at 10x magnification, drawing a line perpendicularly to the interface with pars nervosa up to the pars distalis, sometimes ending at the remnants of Rathke's pouch. Obvious tangential areas were avoided, and thinnest distances were measured. Undulations projecting into the pars nervosa were evaluated subjectively.

2.6. Data Analysis. Data were analyzed using SAS 9.1 (SAS Institute, Cary, NC) and SigmaPlot 2000. Means and standard errors of the means were determined by genotype, gender, and age using the General Linear Model for Vd parameters. Mean thickness of the pars intermedia, standard errors, and unpaired t-tests were obtained using SigmaPlot. For data shown in bar graphs or tables, n is the number of animals. Results were considered significant when $P \leq .05$. Data points from WT mice were pooled since no significant differences were found in morphometry within age comparisons.

Images were obtained using a Spot I camera and Nikon inverted microscope or scanned from electron microscopy prints. Images were contrast enhanced, and, when needed, the grey tones were evened, and the bandaid, dust, and scratches filters were conservatively applied with Photoshop 7 (Adobe.com), without altering the integrity of the histological data.

3. Results

3.1. Development of Cysts in the Pars Distalis of NHE2-null Mice. Previous studies of *Nhe2*$^{-/-}$ mice revealed functional defects directly related to loss of ion transport activity in stomach, kidney, and colon [12, 15, 16]. Although some disturbances in fertility of *Nhe2*$^{-/-}$ mice were suggested [12], gross appearance, growth curves, and overall health of *Nhe2*$^{-/-}$ mice were seemingly normal. However, in a routine histological survey of H&E-stained tissues, we observed cyst-like structures in the pars distalis of *Nhe2*$^{-/-}$ pituitary glands (Figure 1). These first became noticeable by 5 weeks of age and by 10 weeks were well developed. Such cystic changes could be due to increased secretion of ions and fluid into canalicular spaces or to reduced absorption.

3.2. NHE2 Is Expressed in Pituitary and at the Highest Levels in Pars Distalis. To determine whether the cysts were a direct effect of the loss of NHE2, an absorptive Na^+/H^+ exchanger [15, 16], in pituitary rather than an indirect effect of pathology in other organs, the expression of NHE2 in the pituitary gland was analyzed by blot hybridization and *in situ* hybridization.

Northern blot analysis of pituitary and colon RNA (Figure 2) showed that NHE2 mRNA is expressed in the pituitary, but at much lower levels than in colon, the tissue in which the highest levels of NHE2 are expressed [11]. The relative levels of expression suggest that expression of NHE2 mRNA might be restricted to a limited area of the pituitary or to a small subset of pituitary cells. *In situ* hybridization (Figure 3) showed three distinct areas in coronal and transverse sections from both WT and *Nhe2*$^{-/-}$ mice, comprising the more or less concentrically arranged view of these anatomical divisions, with pars distalis forming the outer layer and pars intermedia in a semicircular array around the centrally located pars nervosa (Figure 3).

In situ hybridization using the antisense probe demonstrated similar grain distribution patterns for both WT and *Nhe2*$^{-/-}$ pituitaries, though the latter signal was greatly reduced in intensity. The antisense probe was complementary to the part of the mRNA that encoded amino acids 684–813 of the protein. This region is present in the mutant mRNA, which contains a frame-shift mutation just beyond codon 172 [12]; it is expressed at low levels in some tissues [12], likely accounting for the reduced signals detected. Hybridization with a control sense probe labeled the entire pituitary uniformly, and at very low levels, with no specific signal in any region (data not shown). With the antisense probe, grain deposition was the highest in the pars distalis, with lower levels in the pars intermedia. In pars distalis, the pattern of distribution of the grains was not clearly specific to either FS cells or to granule cells; however, this may be due to the interdigitation of FS cell cytoplasmic projections around the granule cells. Attempts to determine the membrane location of NHE2 protein by immunolocalization were unsuccessful.

Cystic changes were not observed in pars intermedia or pars nervosa of *Nhe2*$^{-/-}$ or WT mice. The pars intermedia of *Nhe2*$^{-/-}$ mice showed significant thinning (Figure 3, cf. 3(i) and 3(j)) compared to that of WT mice (*Nhe2*$^{-/-}$: $96 \pm 8\,\mu$m, $n = 6$; WT: $146 \pm 8.4\,\mu$m, $n = 5$; $P = .003$). Finger-like projections of the pars intermedia into the pars nervosa (black arrows in Figures 3(e) and 3(g)) appeared to be reduced in *Nhe2*$^{-/-}$ mice as well. These data show that pars intermedia is also affected, although the loss of NHE2

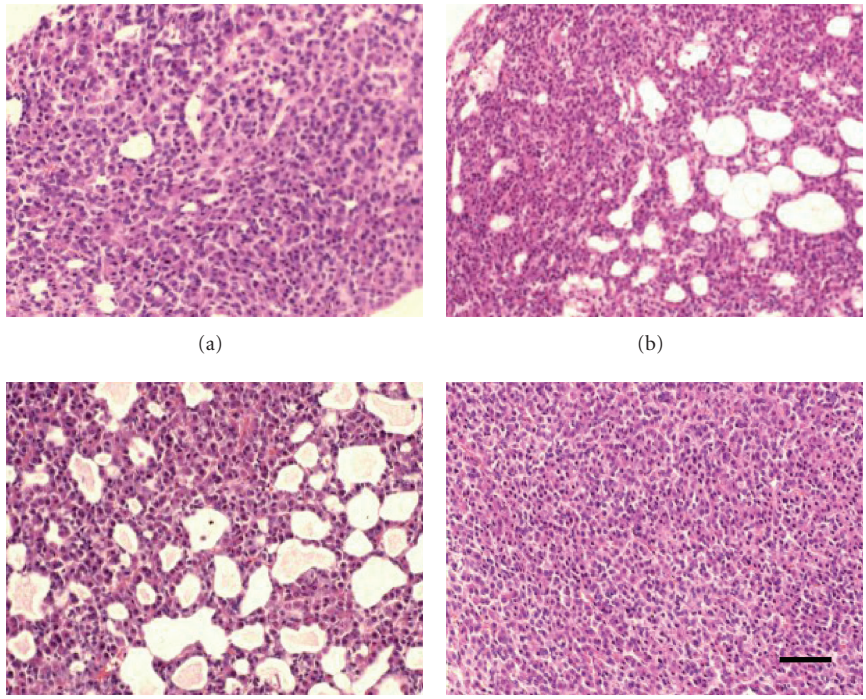

Figure 1: Cystic changes develop with age in the pars distalis of *Nhe2*$^{-/-}$ mice. H&E stained sections of *Nhe2*$^{-/-}$ pituitaries were examined at the following ages: (a) 5 weeks, (b) 8 weeks, and (c) 10 weeks. Note the presence of dilated canaliculi (open spaces) at 8 weeks and 10 weeks. No cyst-like dilatations of the canaliculi were seen in the WT mice at 10 weeks (d) or earlier ages (not shown). Bar: 20 μm.

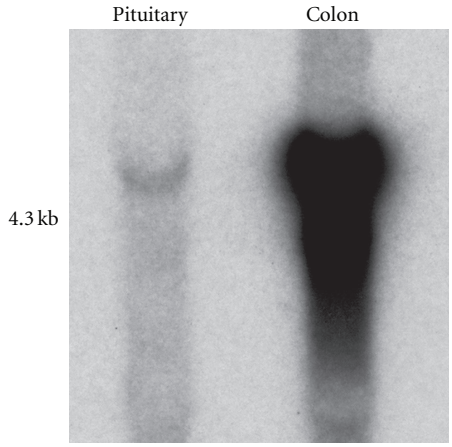

Figure 2: Northern blot analysis of NHE2 mRNA in pituitary and colon. Each lane contained 20 μg of total RNA from WT tissues. Hybridization with a rat NHE2 cDNA probe, which exhibited 93% identity to the mouse sequence and spanned the coding region of the gene, identified the expected 4.3 kb mRNA.

did not cause cystic changes as in pars distalis, at least in the time frame studied.

3.3. Light and Electron Microscopy and Morphometry. FS cells and their junctional complexes formed the canaliculi. On tissue sections they occupied a very small percent of the pars distalis in WT mice, a volume density (Vd) of less than 2%. Canalicular lumens were generally collapsed in WT mouse pituitary but on occasion canaliculi contained small amounts of membrane-like debris. In contrast, in *Nhe2*$^{-/-}$ mice there was a considerable increase in the combined Vd of FS cells and canalicular space (Figure 4) to a Vd of more than 10% (NHE2 null: 12.05% ± 2.9; WT: 1.45% ± 0.35). The integrity of the canalicular lumens seemed not to be compromised, but it became apparent that with increasing age the combined Vd of FS cells and follicular space (Figure 4) increased in the pars distalis. The dilation of canaliculi began in young adulthood and was striking at one year. Analysis of pituitary sections from a single 56-day old achlorhydric mouse that lacked the gastric H^+, K^+-ATPase α subunit [14] revealed no histopathology.

The Vd of large granule pituitary cells (somatotrophs + mammotrophs) was greater in *Nhe2*$^{-/-}$ pituitaries (Figure 4) compared to WT. However, no differences were detected in the actual morphology of the large granule cells. Both Vd of FS cells (Figure 5) and dilation of canaliculi gradually increased in *Nhe2*$^{-/-}$ mice compared to WT (Figure 5). And while the Vd of FS cell cytoplasm and nucleus increased to about 4% in the aged *Nhe2*$^{-/-}$ mice ($P = .04$) it still represented only a small portion of the pars distalis as a whole. The increase in the Vd of FS cells appeared to be FS cell hypertrophy rather than hyperplasia; this backed up the fact that there was no statistically significant increase in the number of mitotic cells in the *Nhe2*$^{-/-}$ mice (*Nhe2*$^{-/-}$: 0.022 ± 0.17; WT: 0.003 ± 0.02, $P = .48$).

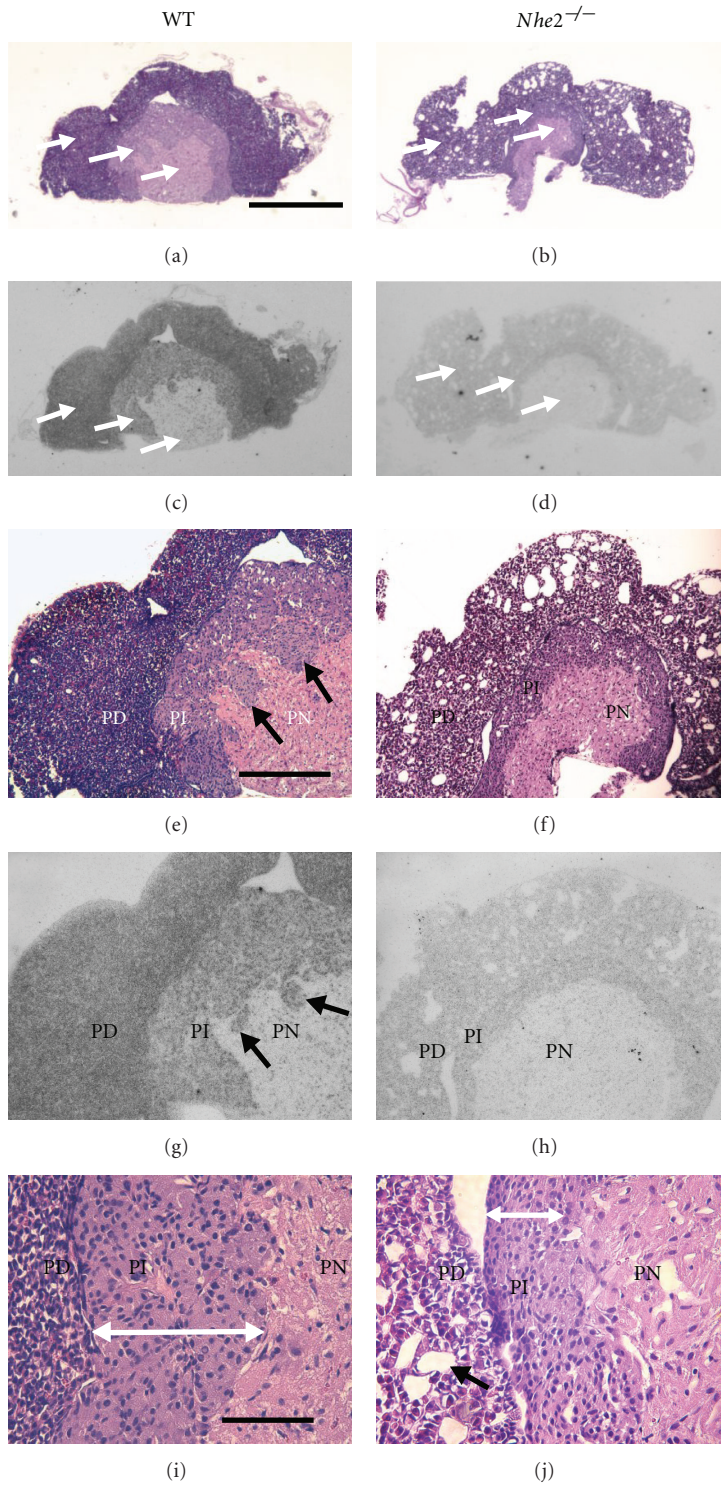

Figure 3: *In situ* hybridization analysis of NHE2 mRNA expression and histology. (a), (c) and (b), (d) are paired serial light micrographs of WT and $Nhe2^{-/-}$ pituitary, H&E-stained and *in situ* hybridization using the antisense probe (resp.). Hybridization with the sense probe yielded no specific signal in either WT or $Nhe2^{-/-}$ samples (data not shown). Three distinct areas of the pituitary are visible in both genotypes (white arrows) at 2x magnification. (e), (g) and (f), (h) are similar pairs at 10x showing that the most dense grain deposits were over the pars distalis (PD), less grain density over the pars intermedia (PI), and much lower grain density over the pars nervosa (PN). Black arrows in (e) and (g) indicate projections from the PI into the PN. The grain deposition over the PI demonstrated a distinct glandular (tubular) arrangement. (i) and (j) are paired WT and $Nhe2^{-/-}$ H&E stained sections at 40x where the difference in thickness of the PI (double headed white arrows) is clear. Cystic dilations (open spaces) of the FS cell canaliculi are clearly apparent in the PD of the $Nhe2^{-/-}$ mice ((b), (d), (f), (h), and (j)); bars : 750 μm in (a)–(d), 40 μm in (e)–(h), and 10 μm in (i) and (j).

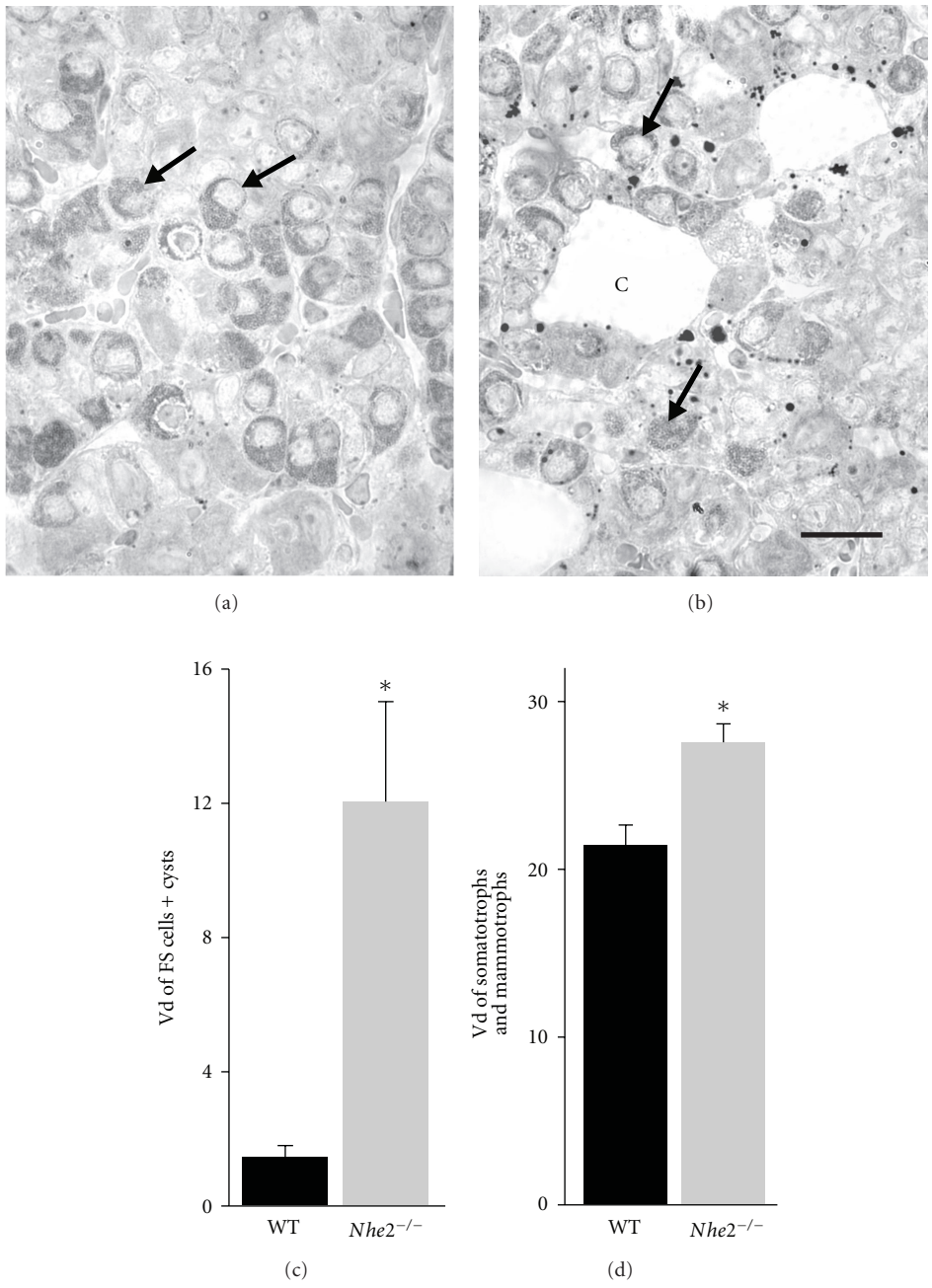

FIGURE 4: Loss of NHE2 leads to increased Vd of both FS cells + cystic dilations (combined) and large granule cells. (a) and (b) are toluidine blue stained sections of pars distalis from WT and *Nhe2*$^{-/-}$ pituitaries. Arrows point to large granule cells (mainly somatotrophs and mammotrophs). Cystic dilations of FS cell canaliculi (C) developed with the loss of NHE2 and increased in size with age. Bar: 20 μm for both WT and *Nhe2*$^{-/-}$. When morphometric data ((c), (d)) for *Nhe2*$^{-/-}$ ($n = 9$) and WT ($n = 7$) mice of all ages were considered, the Vd of the canalicular space plus FS cell nuclei and cytoplasm was significantly greater in *Nhe2*$^{-/-}$ than in WT; $^*P = .0079$. The Vd of large-granule cells also increased significantly in *Nhe2*$^{-/-}$ mice; $^*P = .0026$.

While the Vd of folliculo-stellate cells increased in *Nhe2*$^{-/-}$ mice, in several other respects, FS cell morphology and ultrastructure were similar to those of WT FS cells (Figure 5). Connections among FS cells surrounding the dilatations were seemingly occlusive, and there was no evidence for expansion or edema in the lateral (intercellular) spaces. Junctional complexes were prominent and extensive and, like desmosomes, were most common just beneath the canalicular lumens. Canalicular cystic dilatations were quite variable in size and were clearly demarcated by contiguous FS cells. *Nhe2*$^{-/-}$ mice had FS cell canaliculi lined with unremarkable microvilli and an occasional primary cilium and sometimes contained membrane-like fragments and other cellular debris, and recognizable apoptotic bodies. There

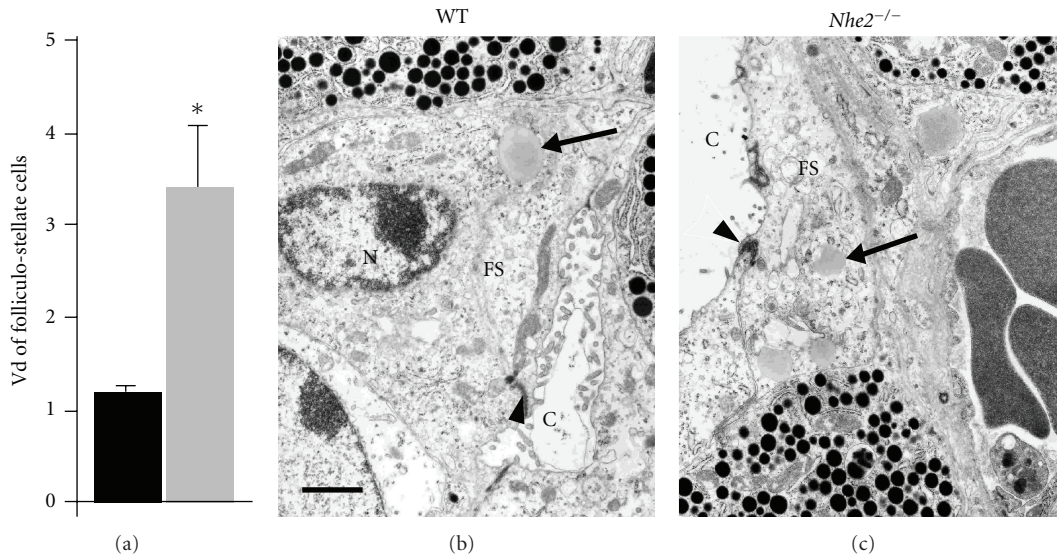

FIGURE 5: *Nhe2*$^{-/-}$ FS cells exhibited increased Vd but relatively normal ultrastructure. (a)**:** morphometric data from the same animals and tissue sections used in Figure 4 showed a significant increase in the Vd of FS cells (cytoplasm + nucleus) in the *Nhe2*$^{-/-}$ pars distalis (*P = .013). Electron microscopy of WT and *Nhe2*$^{-/-}$ FS cells revealed normal ultrastructure except for an increase in lipid droplets (arrows) and decrease in desmosomal-mitochondrial associations (see Figures 6 and 9, resp.). FS cell junctional complexes (arrowheads) were numerous but seemingly unchanged by the loss of NHE2. Note the expanded canalicular space (C) in the *Nhe2*$^{-/-}$ micrograph; FS: folliculo-stellate cell; N: FS cell nucleus; arrows: lipid droplets; bar: 20 μm.

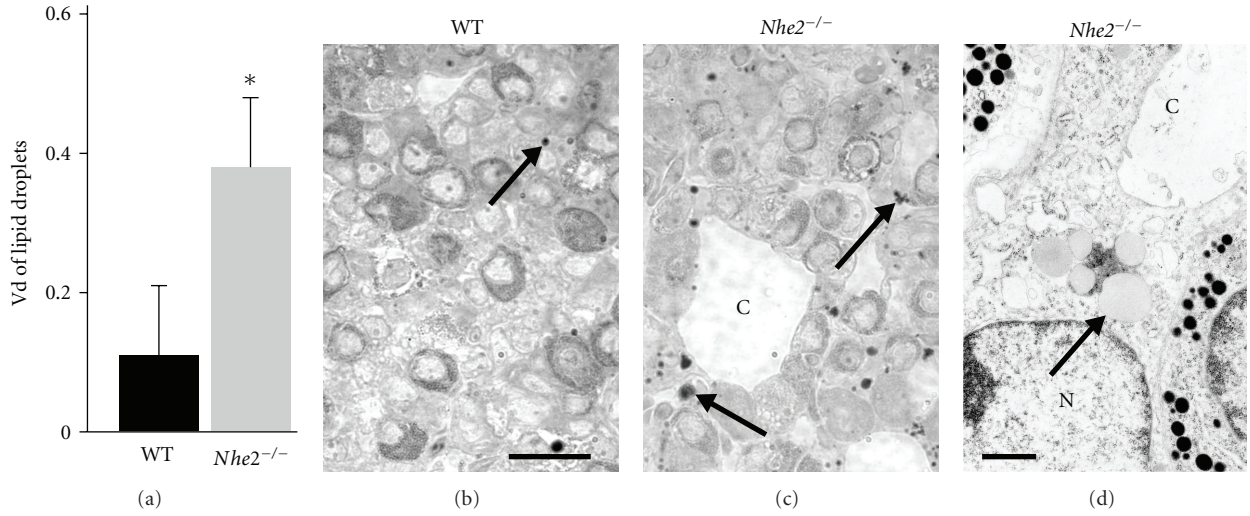

FIGURE 6: The Vd of lipid in FS and other cells in pars distalis was significantly increased. (a): morphometric data from the same animals and tissue sections used in Figure 4 showed a significant increase in the Vd of lipid droplets in *Nhe2*$^{-/-}$ mice when age groups were combined (*P = .0001), but was particularly striking in older *Nhe2*$^{-/-}$ mice. (b) and (c) are light micrographs, for which the bar is 20 μm; (d) is an electron micrograph, bar: 1 μm. Black arrows point to lipid droplets; C: canalicular space; N: nucleus.

were occasional phagolysosmal structures within FS cells, particularly in the *Nhe2*$^{-/-}$ mice. Ultrastructure of the FS cell cytoplasm and nucleoplasm was not obviously changed in organization (Figure 5), and intercellular interdigitations among FS cells, appearance of the rough endoplasmic reticulum, polyribosomes, mitochondria, Golgi bodies, nuclei, and other organelles appeared to be unchanged from WT as well. The exception was the accumulation of lipid droplets.

An increase in small lipid droplets (Figure 6) was found predominantly in FS cell cytoplasm, and also in other cell types, including granulated cells. The Vd of lipid was about 3-fold greater in the aging *Nhe2*$^{-/-}$ mice than in WT mice, but in both groups the Vd of lipid increased as age increased. Values for Vd of lipid for each group were compared with the genotype-matched younger age group (resp.), but statistical significance was reached in the

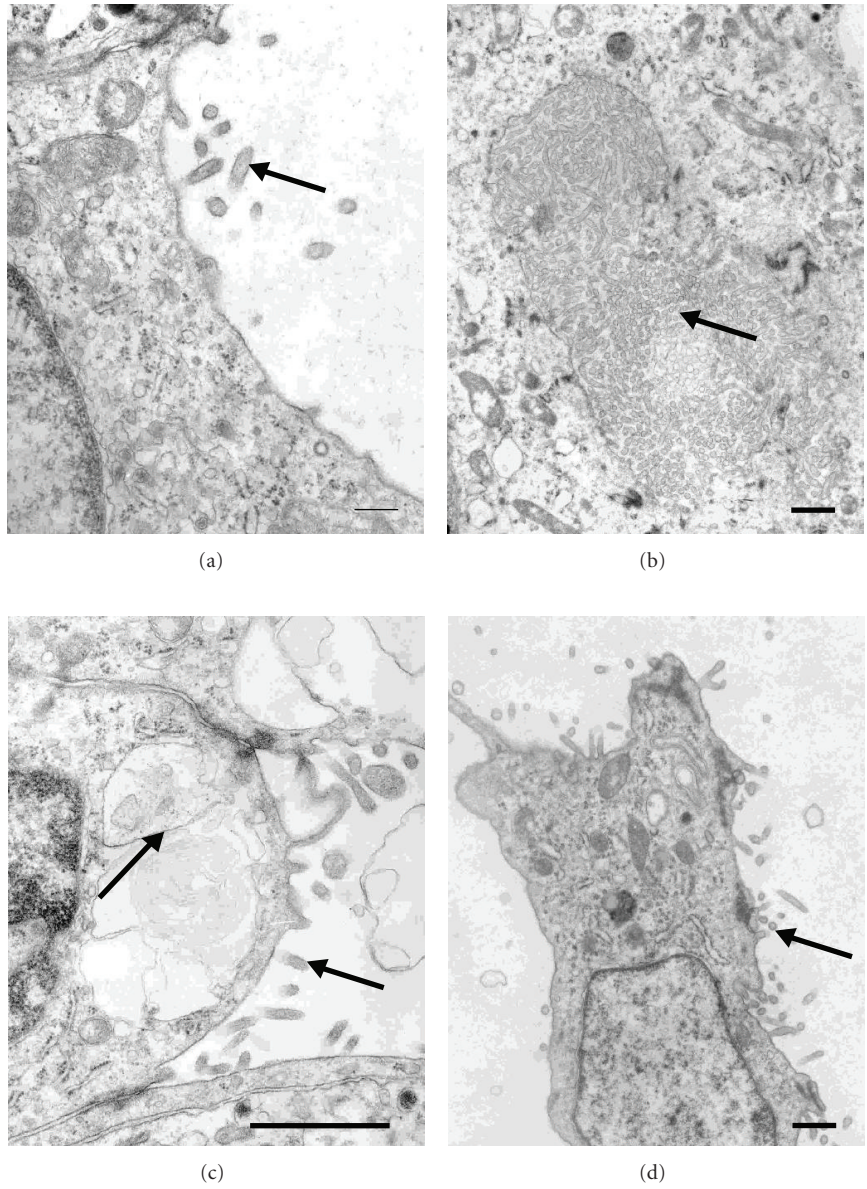

Figure 7: Microvilli on the apical membrane of FS cells of WT and *Nhe2*$^{-/-}$ mice were similar morphologically. Electron micrographs of (a) WT and (b)–(d) *Nhe2*$^{-/-}$ FS cells. Arrowheads point to microvilli. Dense patches of tightly packed microvilli were occasionally seen in FS cell canaliculi in the null animals; in (b), the arrowhead lies in the center of one such canaliculus. Cytoplasmic vacuoles in the apical cytoplasm of FS cells sometimes had membranous inclusions, as indicated by the arrow in (c). C: canaliculus; N: nucleus; bars: 1 μm.

Nhe2$^{-/-}$ animals only. Lipid droplets were typically less than a few μm in diameter and were found either as part of or adjacent to inclusions (phagolysosomes or autophagosomes) (Figure 6(a)).

Microvilli on the apical membranes of FS cells of *Nhe2*$^{-/-}$ mice (projecting into the canalicular space) were not noticeably different from WT (Figure 7). They appeared similar to the flexible microvilli that were found in numerous other tissues, such as bile canaliculi in the liver and canalicular microvilli of parietal cells in the stomach (about 1 μm in length). The actin filaments seen on cross-section were more or less evenly distributed within the microvillus, if not peripherally, and were definitely not bundled centrally as one typically sees in intestinal and renal brush border. The microvilli were not very densely packed along the FS cell apical membrane in either WT or *Nhe2*$^{-/-}$ FS cells (Figure 7) though, on occasion, areas of densely packed microvilli were found in the *Nhe2*$^{-/-}$ FS cells displaying a phenotype not unlike that of parietal cell canaliculi. Similar to the membrane-like debris occasionally found in canalicular lumens, membrane-like debris was sometimes found within the apical cytoplasm of FS cells of *Nhe2*$^{-/-}$ mice (Figure 7). The Vd of these areas was not quantified with light microscopy.

Basal membranes of FS cells adjacent to capillary endothelium abutted two basement membranes: one an FS

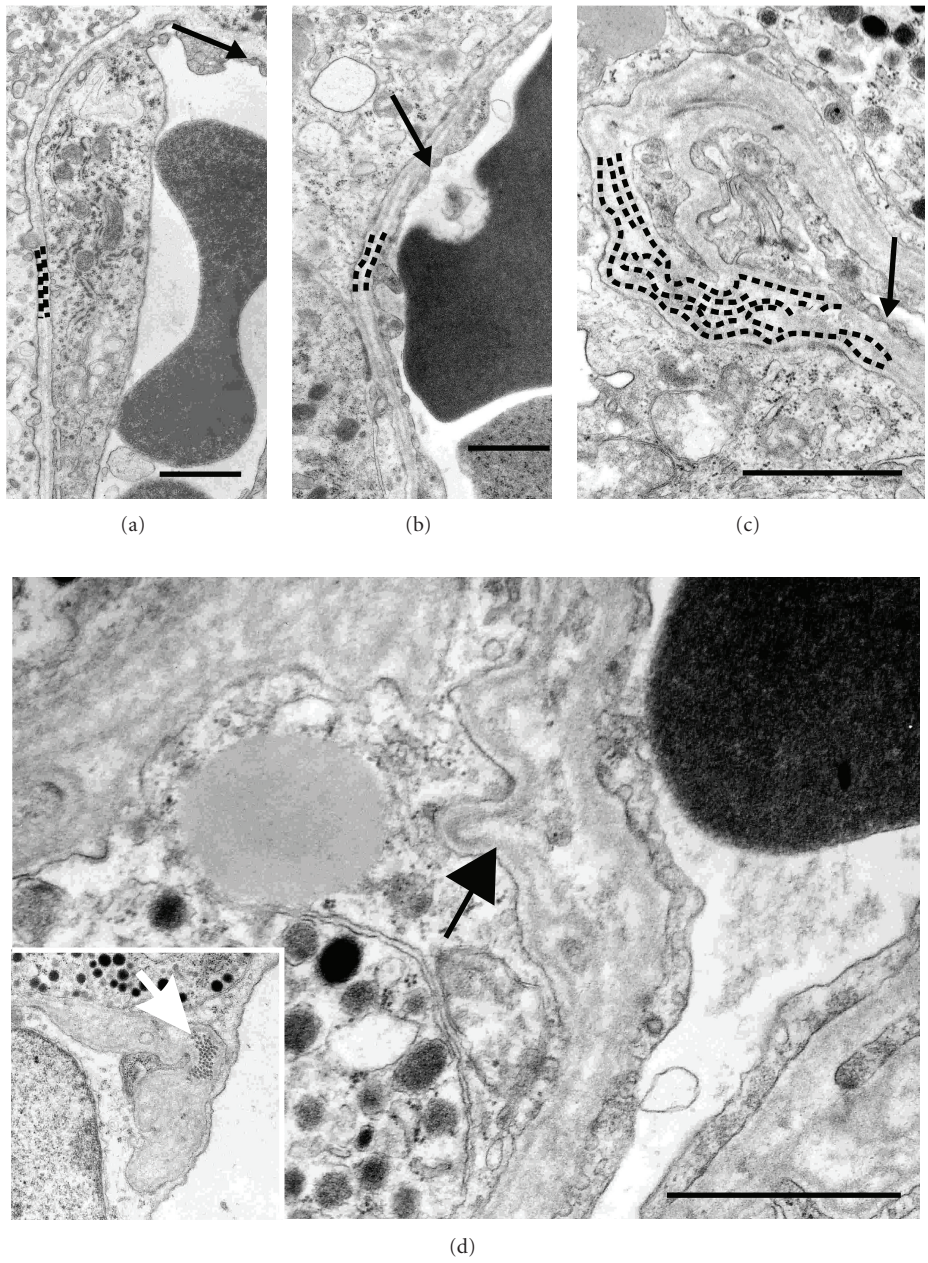

Figure 8: Duplicated and redundant basement membranes were found in *Nhe2*$^{-/-}$ pars distalis. In WT pars distalis (a) there are two parallel basement membranes between capillary endothelial cells and FS cells, one from each cell type. Similar parallel basement membranes were observed in some *Nhe2*$^{-/-}$ electron micrographs (b), but in conspicuous spots the basement membrane appeared to be duplicated and/or redundant in *Nhe2*$^{-/-}$ mice, which was particularly evident proximate to the FS cells ((c) and (d)), as indicated by the arrowhead in (d). Dotted lines overlay basement membranes. (a)–(c) black arrows point to fenestrated capillaries, which apparently did not change in *Nhe2*$^{-/-}$ mice. L: lipid droplet. Inset: white arrow, collagen. Bars: 1 μm.

cell product and the other produced by the capillary endothelium. In WT mice these two were largely parallel (Figure 8). Reduplicated and redundant basement membranes were common in the *Nhe2*$^{-/-}$ mice, older animals showing greater changes. Redundancies were sometimes focal, and on occasion as many as 8 redundancies were counted, with a mean number of basement membranes in the *Nhe2*$^{-/-}$ samples significantly greater than in WT (WT: $n = 3$, 1.7 ± 0.19; *Nhe2*$^{-/-}$: $n = 4$, 2.2 ± 0.14, $P = .036$). Subjectively, areas of redundant and duplicated membrane appeared more likely to be attributable to the FS cells than to the capillary endothelium. An increase in other extracellular matrix proteins may have occurred as well, and occasionally collagen was seen.

The Vd of blood vessels in the pars distalis was not significantly different among the groups of old, young, null, or WT mice. Blood vessels represented about 4.5% of the Vd of the pars distalis.

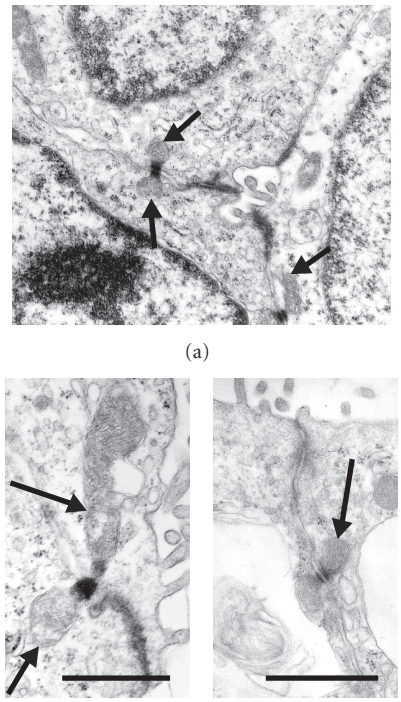

Figure 9: *Nhe2*$^{-/-}$ FS cells exhibited a reduction in the number of desmosomes associated with mitochondria. Desmosomal-mitochondrial associations can be seen in WT ((a) and (b)) and in *Nhe2*$^{-/-}$ mice (c). Desmosomes are often associated with one or two mitochondria (one from each cell). A significant decrease in desmosomal-mitochondrial associations was found in the FS cells of *Nhe2*$^{-/-}$ mice (see Table 1). Arrows point to mitochondria whose outer membranes are juxtaposed to intracellular filaments of desmosomes. Bars: 1 μm.

There were many desmosomal-mitochondrial connections, which spanned adjacent FS cell membranes at the site of desmosomes (Figure 9). These comprise mitochondria with a portion of outer lamella abutting the keratin filaments which radiate from the desmosome into the cytoplasm. Such desmosomal-mitochondrial juxtapositions often were present on both sides of the desmosome (i.e., adjacent to desmosomes in adjacent cells), other times adjacent to the desmosome on one side only. Since so many of these juxtapositions occurred, they are likely more paired than not, at least in WT mice, and section orientation has left one mitochondrion unseen (Table 1). The order and incidence of junctional complexes, desmosomes, and desmosomal-mitochondrial associations in a tally made from electron micrographs revealed a significant reduction from WT in the number of desmosomes which were associated with 2 mitochondria (Table 1).

Junctional complexes, intercellular spaces, membrane interdigitations, microvilli, and pinocytotic vesicles/caveolae are not different in *Nhe2*$^{-/-}$ than in WT samples, as counted in this study. A count of caveolae per membrane profile per cell showed no significant difference between WT and *Nhe2*$^{-/-}$ (WT: 0.69 ± 0.16; *Nhe2*$^{-/-}$: 0.23 ± 0.10; $P = .2$).

4. Discussion

The most prominent histological finding consequent to gene-targeted ablation of the NHE2 Na^+/H^+ exchanger was the dilation of the canaliculi formed by FS cells in the pars distalis of the anterior pituitary. The cyst-like structures were lined by FS cells, with their luminal surfaces containing microvilli, and a morphology clearly indicating that they were derived from the network of interconnected follicular cavities. Such structures have been reported to extend throughout the anterior pituitary [2]. The cysts became apparent at about 5 weeks of age and were very prominent by 8 and 10 weeks. The absence of cysts in pituitary sections from an achlorhydric mouse lacking the gastric H^+,K^+-ATPase α subunit indicated that the cysts in the *Nhe2*$^{-/-}$ pituitaries were a direct response to the loss of NHE2 in the pituitary rather than an indirect response to achlorhydria. Given the known absorptive functions of NHE2 [14, 15], the expression of NHE2 mRNA in pars distalis and at lesser levels in pars intermedia, both of which are reported to contain FS cells, and the previously demonstrated transcellular fluxes of ions and water across FS cells [4, 5], the data suggest that NHE2 serves as an important absorptive Na^+/H^+ exchanger on the luminal surface of FS cells of the anterior pituitary.

NHE2 mRNA expression, as indicated by Northern blot analysis, was very low in the pituitary gland when compared with its expression in colon [15], the tissue with the highest expression in rats and mice [11, 12]. The apparent low level of expression may be due in part to the relatively low abundance of FS cells compared to endocrine cells, as indicated by measurements of FS cell Vd; however, other factors might also be involved. Under normal conditions, the luminal membrane of the follicles, where NHE2 is presumably expressed, is a small percentage of the total plasma membrane of FS cells. In addition, the gradual appearance and expansion of the canaliculi in NHE2-null pituitary glands suggest that the absorptive process is far less robust than in colonic crypts and kidney, where large quantities of ions and water are absorbed on a continuous basis. Rather, the pituitary phenotype developing with the loss of NHE2 suggests that absorption mediated by low levels of NHE2 may counter relatively low levels of fluid accumulation in the follicular cavities. Attempts to identify the membrane location of NHE2 protein in the pituitary gland using antibodies that have been used for immunolocalization in apical membranes of salivary acinar and duct cells [19] were unsuccessful. Thus, at the present time the membrane location of NHE2 can only be inferred from the histological phenotype and from its expression on apical membranes in epithelial tissues where it is expressed at much higher levels.

Earlier studies showed that FS cells in culture can function like typical epithelial cells involved in transepithelial ion and fluid transport. When grown as primary cultures, FS cells derived from the pars distalis and pars tuberalis [4] and from the pars intermedia [5] formed domes, indicating that they absorbed ions and water from the culture fluid. Studies using cultured cells mounted in Ussing chambers [5] showed that application of β-adrenergic

Table 1: Percentage of desmosomes associated with at least one mitochondrion in FS cells.

WT		*Nhe2*$^{-/-}$	
% Desmosomes with at least 1 mitochondrion	% Desmosomes with 2 mitochondria	% Desmosomes with at least 1 mitochondrion	% Desmosomes with 2 mitochondria
66.0 ± 23.0	52.3 ± 11.2	12.1 ± 2.5, $P = .08$*	7.1 ± 3.6, $P = .02$*

Desmosomal-mitochondrial associations in FS cells from WT and *Nhe2*$^{-/-}$ mice ($n = 3$ for each group) were analyzed by electron microscopy. Note that the desmosomes associated with two mitochondria (one from each FS cell) are a subset of those associated with at least 1 mitochondrion. *P values are relative to corresponding WT control.

agonists to the serosal surface led to currents consistent with CFTR-mediated anion secretion, whereas application of amiloride to the mucosal surface, at concentrations known to inhibit the epithelial Na^+ channel, led to a reduction in transepithelial currents, with a further reduction in response following inhibition of the Na^+,K^+-ATPase with ouabain. These data indicated that FS cells contained an apical anion channel and apical transporters that were able to absorb Na^+, with accompanying anions, from the luminal spaces. Aquaporin 4 has also been shown to be expressed in FS cells [6], suggesting that it contributes to water transport associated with ion movements. The identities of specific ion transporters involved in transcellular ion fluxes in FS cells have not been determined; however, a recent study showed that CFTR is expressed in the pituitary [16] and the current data indicate that NHE2 plays a critical role in this process.

NHE2 is one of two absorptive Na^+/H^+ exchangers in apical membranes of renal and intestinal epithelial cells [14, 15]. NHE3 mediates high levels of NaCl absorption via coupling with either Cl^-/formate exchange [20] or Cl^-/HCO_3^- exchange [21, 22]. However, when operating alone, Na^+/H^+ exchange mediates Na^+ and HCO_3^- absorption. NHE2 has an unusual pH sensitivity that would appear to make it suitable for a role in $NaHCO_3$ absorption. Its activity is very low at normal extracellular pH, but it exhibits 50% activity at pH 8.0, and its activity increases further as the extracellular pH increases [23]. In the kidney, NHE2 plays a role in Na^+ and HCO_3^- absorption and is particularly important under conditions of increased delivery of HCO_3^- to the distal nephron [14]. In colon, NHE2 is expressed primarily in the crypts [15], where the luminal pH is relatively alkaline in the presence of physiological concentrations of short-chain fatty acids [24], again consistent with a function in $NaHCO_3$ absorption. As far as we are aware, the pH and HCO_3^- content of follicular fluid is not known, but it is possible that the sensitivity of NHE2 to extracellular pH makes it more suitable for its role in the pituitary.

Cystic dilatations were not observed in the pars intermedia of *Nhe2*$^{-/-}$ mice despite the presence of FS cells and NHE2 expression in this segment of WT pituitary glands. The basis for this difference is unclear. It is possible that secretory processes that expand the canaliculi, which may involve CFTR-mediated anion secretion [16], are less active in this segment than in the pars distalis or that a compensatory absorptive mechanism prevents their expansion. For example, an ion transport mechanism that can compensate for the loss of NHE2 has been shown to be activated in colonic crypts of *Nhe2*$^{-/-}$ mice [15]. Alternatively, processes other than absorption or secretion may prevent excessive accumulation of fluid. For example, De Bold et al. [25] reported the presence of two types of interconnected channels in the pars intermedia, which they noted was highly avascular and presumed that fluid and solutes in the channel systems can reach the general circulation. If this were the case, it could provide drainage, thus preventing cyst formation.

It is difficult to draw clear parallels between the pituitary and stomach phenotypes of NHE2-null mice. NHE2 was originally proposed to function on the basolateral membrane of the parietal cell, operating in concert with the AE2 Cl^-/HCO_3^- exchanger to mediate Na^+ and Cl^- uptake that is required for stimulated acid secretion [12]. However, it is clear that the few mature *Nhe2*$^{-/-}$ parietal cells were able to secrete high levels of acid [12] and there is evidence that NHE4 is the basolateral Na^+/H^+ exchanger required for acid secretion [26]. An alternative possibility is that NHE2 is expressed in canalicular membranes, where it could operate in concert with the Slc26a6 Cl^-/HCO_3^- exchanger [27] and other transporters to dehydrate secretory membranes during transitions to the resting state. Such a function would be similar to the absorptive function proposed in FS cells and consistent with its apical expression in other epithelial tissues [14, 15, 19, 28].

The cystic dilations in the FS cell canaliculi in *Nhe2*$^{-/-}$ mice did not readily conform to those of known human or animal pituitary disease, where most reported cystic changes were within pituitary neoplasms or were cysts containing mucins or colloid-type inclusions [29, 30]. Metaplastic transformation of FS cells, described in human pituitary [31], was not found in the *Nhe2*$^{-/-}$ mice. While neither colloid contents nor mucins were found with any regularity within the dilated canaliculi of *Nhe2*$^{-/-}$ (or WT) pituitaries, membrane and nuclear debris were seen on occasion. They were greater in quantity in *Nhe2*$^{-/-}$ pituitaries than in WT, and likely the residue from an occasional expulsion of previously phagocytosed apoptotic debris into the canalicular lumen. The amount of cellular debris, apoptotic bodies, or phagolysosomal vacuoles did not suggest excessive FS cell death in the *Nhe2*$^{-/-}$ mice. This is in contrast to conspicuous parietal cell death which occurred in the stomach of *Nhe2*$^{-/-}$ mice [12].

FS cell microvilli most closely resembled the morphology of bile canaliculi in the liver, but *Nhe2*$^{-/-}$ FS cells occasionally formed apical invaginations containing clusters of densely packed microvilli (Figure 7(b)) resembling those of parietal cell canaliculi [13]. It is unclear whether these rare instances

of densely packed microvilli correspond to an absorptive state or to a secretory state, as is the case for parietal cells, but given the invagination of the canaliculus into the cell a secretory state seems more likely.

Ultrastructure was also affected on the basal side of FS cells and comprised duplicated and/or redundant basement membranes. FS cells produce their own basement membranes, of the "continuous" type, distinct from, and parallel to, basement membranes of the capillary bed. The ability of these cells to produce matrix proteins and basement membrane structures has been described using a transgenic mouse model [32]. Redundancies in basement membranes occurred primarily beneath FS cells and were short and fragmented. Duplicated basement membranes have been described in bile duct [33] and other tissues [34–36] but were not reported in stomach or other affected tissues of the *Nhe2*$^{-/-}$ mouse [12, 13]. It is possible that physical strain related to canalicular dilation could induce an increase in matrix proteins or that perturbations of cellular homeostasis related to the ion transport defect are involved.

FS cells displayed numerous instances of close physical associations between mitochondria and the intracellular filaments of desmosomes. In WT mice, over half of the desmosomes exhibited associations with two mitochondria, one from each cell contributing to the desmosomal junction. *Nhe2*$^{-/-}$ FS cells exhibited a significant decrease in the percentage of desmosomes associated with 2 mitochondria, from 52% in WT to 7% in mutant mice. Desmosomes undergo frequent remodeling [37], so if mitochondria are involved in this process, it would suggest less remodeling in *Nhe2*$^{-/-}$ FS cells. The frequent associations between mitochondria and desmosomes have led to speculations of their providing for energy requirements and calcium delivery, but the function is not known. These desmosome-mitochondria associations [38–41] lend further credence to the dynamic nature of the apical membrane of FS cells.

Lipid droplet accumulation in the cytoplasm of cells is a well-recognized indicator of cell stress and pathology [42–45]. Therefore the significant increase in cytoplasmic lipid in FS and granule cells of the pars distalis of *Nhe2*$^{-/-}$ mice may be an indication of cell stress resulting from the loss of NHE2. This observation and the increased Vd of large granule cells indicate that these endocrine cells are negatively affected by the FS cell defect.

The function of the canalicular network is unclear [2]; however, there is compelling evidence that FS cells themselves form an extensive cell network in addition to the canalicular network and that intrapituitary communication occurs via Ca^{2+} signaling through gap junctions [9, 10, 46–48]. This mechanism, which allows propagation of Ca^{2+} signals over long distances within the anterior pituitary, has been suggested to provide a means by which FS cells synchronize secretory activity of endocrine cells [9, 10]. It is clearly important, and perhaps predominant; however, it has also been noted that the anastomosing channels formed by FS cells [2] might provide a means of synchronizing hormone secretion [10]. One can speculate that the two networks operate separately, with FS cell Ca^{2+} signaling through gap junctions providing rapid coordination of endocrine activity and FS cell control of the canalicular fluid composition via ion secretion and absorption providing longer-term regulation. Alternatively, anion secretion and Ca^{2+} signaling might act in concert if they were stimulated together or if one activity triggered the other. Additional studies will be needed to identify all of the transporters involved in ion secretion and absorption by FS cells and to determine their relevance to human diseases involving transepithelial ion transport defects. In this regard, it has long been reported that pituitary function is impaired in cystic fibrosis, the most common genetic disease in humans, and recent work showed that CFTR is expressed in pituitary and that the absence of its activity impairs hormone secretion ([16], and references therein).

In conclusion, the loss of NHE2 produced anterior pituitary pathology, including a gross dilation of FS cell canaliculi, increase in the Vd of FS cells, a significant accumulation of small lipid droplets in FS cell and granule cell cytoplasm, a reduction in desmosomal-mitochondrial complexes, reduplication of the FS cell basement membranes, an increase in the Vd of somatotrophs and mammotrophs, and a thinning of the pars intermedia. The absence of apparent effects on growth and development [12] suggests that dilation of the canaliculi resulting from the loss of NHE2 is a relatively benign defect. Nevertheless, a fertility defect [12] remains unexplained, and the increase in both Vd and lipid droplets in large granule cells showed that endocrine cells are affected. The dilation of the canaliculi suggests that NHE2 is the major absorptive mechanism that counters the accumulation of canalicular fluid resulting from ion secretion by FS cells. Thus, if ion secretion serves an important function in the pituitary, as suggested by studies on the pig cystic fibrosis model and human infants with cystic fibrosis [16], then one might expect that disease conditions or drugs that impair ion secretion or homeostatic regulation of the volume and ionic composition of the canalicular fluid would affect pituitary function and human health.

Acknowledgments

This research was funded in part by NIEHS P30-ES006096 and R01 DK050594. The authors thank Angel Whittaker and Maureen Bender for expert animal husbandry.

References

[1] D. C. Herbert and A. Y. Silverman, "Topographical distribution of the gonadotrophs, mammotrophs, somatotrophs and thyrotrophs in the pituitary gland of the baboon (Papio cynocephalus)," *Cell and Tissue Research*, vol. 230, no. 1, pp. 233–238, 1983.

[2] W. Allaerts, P. Carmeliet, and C. Denef, "New perspectives in the function of pituitary folliculo-stellate cells," *Molecular and Cellular Endocrinology*, vol. 71, no. 2, pp. 73–81, 1990.

[3] K. Inoue, E. F. Couch, K. Takano, and S. Ogawa, "The structure and function of folliculo-stellate cells in the anterior pituitary gland," *Archives of Histology and Cytology*, vol. 62, no. 3, pp. 205–218, 1999.

[4] N. Ferrara, D. K. Fujii, and P. C. Goldsmith, "Transport epithelial characteristics of cultured bovine pituitary follicular cells," *American Journal of Physiology*, vol. 252, no. 3, part 1, pp. E304–E312, 1987.

[5] N. Ferrara and D. Gospodarowicz, "Regulation of ion transport in hypophysial pars intermedia follicular cell monolayers," *Biochemical and Biophysical Research Communications*, vol. 157, no. 3, pp. 1376–1382, 1988.

[6] S. Kuwahara, S. Maeda, Y. Ardiles et al., "Immunohistochemical localization of aquaporin-4 in the rat pituitary gland," *Journal of Veterinary Medical Science*, vol. 72, no. 10, pp. 1307–1312, 2010.

[7] S. Devnath and K. Inoue, "An insight to pituitary folliculostellate cells," *Journal of Neuroendocrinology*, vol. 20, no. 6, pp. 687–691, 2008.

[8] N. Ferrara, L. Schweigerer, G. Neufeld, R. Mitchell, and D. Gospodarowicz, "Pituitary follicular cells produce basic fibroblast growth factor," *Proceedings of the National Academy of Sciences of the United States of America*, vol. 84, no. 16, pp. 5773–5777, 1987.

[9] T. Fauquier, N. C. Guérineau, R. A. McKinney, K. Bauer, and P. Mollard, "Folliculo-stellate cell network: a route for long-distance communication in the anterior pituitary," *Proceedings of the National Academy of Sciences of the United States of America*, vol. 98, no. 15, pp. 8891–8896, 2001.

[10] S. S. Stojilkovic, "A novel view of the function of pituitary folliculo-stellate cell network," *Trends in Endocrinology and Metabolism*, vol. 12, no. 9, pp. 378–380, 2001.

[11] Z. Wang, J. Orlowski, and G. E. Shull, "Primary structure and functional expression of a novel gastrointestinal isoform of the rat Na/H exchanger," *Journal of Biological Chemistry*, vol. 268, no. 16, pp. 11925–11928, 1993.

[12] P. J. Schultheis, L. L. Clarke, P. Meneton et al., "Targeted disruption of the murine Na/H exchanger isoform 2 gene causes reduced viability of gastric parietal cells and loss of net acid secretion," *Journal of Clinical Investigation*, vol. 101, no. 6, pp. 1243–1253, 1998.

[13] M. L. Miller, A. Andringa, Y. Zavros, E. M. Bradford, and G. E. Shull, "Volume density, distribution, and ultrastructure of secretory and basolateral membranes and mitochondria predict parietal cell secretory (Dys)function," *Journal of Biomedicine and Biotechnology*, vol. 2010, Article ID 394198, 13 pages, 2010.

[14] M. A. Bailey, G. Giebisch, T. Abbiati et al., "NHE2-mediated bicarbonate reabsorption in the distal tubule of NHE3 null mice," *Journal of Physiology*, vol. 561, no. 3, pp. 765–775, 2004.

[15] Y. Guan, J. Dong, L. Tackett, J. W. Meyer, G. E. Shull, and M. H. Montrose, "NHE2 is the main apical NHE in mouse colonic crypts but an alternative Na+-dependent acid extrusion mechanism is upregulated in NHE2-null mice," *American Journal of Physiology*, vol. 291, no. 4, pp. G689–G699, 2006.

[16] M. P. Rogan, L. R. Reznikov, A. A. Pezzulo et al., "Pigs and humans with cystic fibrosis have reduced insulin-like growth factor 1 (IGF1) levels at birth," *Proceedings of the National Academy of Sciences of the United States of America*, vol. 107, no. 47, pp. 20571–20575, 2010.

[17] C. Ledoussal, J. N. Lorenz, M. L. Nieman, M. Soleimani, P. J. Schultheis, and G. E. Shull, "Renal salt wasting in mice lacking NHE3 Na^+/H^+ exchanger but not in mice lacking NHE2," *American Journal of Physiology*, vol. 281, no. 4, pp. F718–F727, 2001.

[18] D. M. Simmons, J. L. Arriza, and L. W. Swanson, "A complete protocol for in situ hybridization of messenger RNAs in brain and other tissues with radiolabeled single-stranded RNA probes," *Journal of Histotechnology*, vol. 12, no. 3, pp. 169–181, 1989.

[19] K. Park, R. L. Evans, G. E. Watson et al., "Defective fluid secretion and NaCl absorption in the parotid glands of Na^+/H^+ exchanger-deficient mice," *Journal of Biological Chemistry*, vol. 276, no. 29, pp. 27042–27050, 2001.

[20] T. Wang, C. L. Yang, T. Abbiati, G. E. Shull, G. Giebisch, and P. S. Aronson, "Essential role of NHE3 in facilitating formate-dependent NaCL absorption in the proximal tubule," *American Journal of Physiology*, vol. 281, no. 2, pp. F288–F292, 2001.

[21] J. E. Melvin, K. Park, L. Richardson, P. J. Schultheis, and G. E. Shull, "Mouse down-regulated in adenoma (DRA) is an intestinal Cl^-/HCO_3^- exchanger and is up-regulated in colon of mice lacking the NHE3 Na^+/H^+ exchanger," *Journal of Biological Chemistry*, vol. 274, no. 32, pp. 22855–22861, 1999.

[22] N. M. Walker, J. E. Simpson, P. F. Yen et al., "Down-regulated in adenoma Cl/HCO_3 exchanger couples with Na/H exchanger 3 for NaCl absorption in murine small intestine," *Gastroenterology*, vol. 135, no. 5, pp. 1645–1653, 2008.

[23] F. H. Yu, G. E. Shull, and J. Orlowski, "Functional properties of the rat Na/H exchanger NHE-2 isoform expressed in Na/H exchanger-deficient Chinese hamster ovary cells," *Journal of Biological Chemistry*, vol. 268, no. 34, pp. 25536–25541, 1993.

[24] S. Chu and M. H. Montrose, "Non-ionic diffusion and carrier-mediated transport drive extracellular pH regulation of mouse colonic crypts," *Journal of Physiology*, vol. 494, no. 3, pp. 783–793, 1996.

[25] A. J. De Bold, M. L. De Bold, and J. Kraicer, "Structural relationships between parenchymal and stromal elements in the pars intermedia of the rat adenohypophysis as demonstrated by extracellular space markers," *Cell and Tissue Research*, vol. 207, no. 3, pp. 347–359, 1980.

[26] L. R. Gawenis, J. M. Greeb, V. Prasad et al., "Impaired gastric acid secretion in mice with a targeted disruption of the NHE4 Na^+/H^+ exchanger," *Journal of Biological Chemistry*, vol. 280, no. 13, pp. 12781–12789, 2005.

[27] S. Petrovic, Z. Wang, L. Ma et al., "Colocalization of the apical Cl^-/HCO_3^- exchanger PAT1 and gastric H-K-ATPase in stomach parietal cells," *American Journal of Physiology*, vol. 283, no. 5, pp. G1207–G1216, 2002.

[28] R. Chambrey, D. G. Warnock, R. A. Podevin et al., "Immunolocalization of the Na^+/H^+ exchanger isoform NHE2 in rat kidney," *American Journal of Physiology*, vol. 275, no. 3, part 2, pp. F379–F386, 1998.

[29] H. S. Min, S. J. Lee, S. K. Kim, and S. H. Park, "Pituitary adenoma with rich folliculo-stellate cells and mucin-producing epithelia arising in a 2-year-old girl," *Pathology International*, vol. 57, no. 9, pp. 600–605, 2007.

[30] Y. Kameda, "Occurrence of colloid-containing follicles in the pars distalis of pituitary glands from aging guinea pigs," *Cell and Tissue Research*, vol. 263, no. 1, pp. 115–124, 1991.

[31] E. Horvath, C. I. Coire, K. Kovacs, and H. S. Smyth, "Folliculo-stellate cells of the human pituitary as adult stem cells: examples of their neoplastic potential," *Ultrastructural Pathology*, vol. 34, no. 3, pp. 133–139, 2010.

[32] K. Horiguchi, M. Kikuchi, K. Kusumoto et al., "Living-cell imaging of transgenic rat anterior pituitary cells in primary culture reveals novel characteristics of folliculo-stellate cells," *Journal of Endocrinology*, vol. 204, no. 2, pp. 115–123, 2010.

[33] M. Kage, K. Kosai, K. Shimamatsu et al., "Ultrastructural studies of the bile duct in alcoholic liver disease," *Kurume Medical Journal*, vol. 39, no. 4, pp. 219–229, 1992.

[34] S. S. Sohal, D. Reid, A. Soltani et al., "Reticular basement membrane fragmentation and potential epithelial mesenchymal transition is exaggerated in the airways of smokers with chronic obstructive pulmonary disease," *Respirology*, vol. 15, no. 6, pp. 930–938, 2010.

[35] L. L. Richardson, H. K. Kleinman, and M. Dym, "Altered basement membrane synthesis in the testis after tissue injury," *Journal of Andrology*, vol. 19, no. 2, pp. 145–155, 1998.

[36] T. W. C. Tervaert, A. L. Mooyaart, K. Amann et al., "Pathologic classification of diabetic nephropathy," *Journal of the American Society of Nephrology*, vol. 21, no. 4, pp. 556–563, 2010.

[37] D. Garrod and M. Chidgey, "Desmosome structure, composition and function," *Biochimica et Biophysica Acta*, vol. 1778, no. 3, pp. 572–587, 2008.

[38] J. Rassat, H. Robenek, and H. Themann, "Structural relationship between desmosomes and mitochondria in human livers exhibiting a wide range of diseases," *American Journal of Pathology*, vol. 105, no. 3, pp. 207–211, 1981.

[39] L. H. Bernstein and S. H. Wollman, "Association of mitochondria with desmosomes in the rat thyroid gland," *Journal of Ultrastructure Research*, vol. 53, no. 1, pp. 87–92, 1975.

[40] T. F. Freddo, "Mitochondria attached to desmosomes in the ciliary epithelia of human, monkey, and rabbit eyes," *Cell and Tissue Research*, vol. 251, no. 3, pp. 671–675, 1988.

[41] M. L. Miller, A. Andringa, J. M. Manson et al., "An ultrastructural survey of desmosomal-mitochondrial complexes in the liver of several species of laboratory mammal," *Ohio Journal of Science*, vol. 85, pp. 74–84, 1985.

[42] I. Barba, M. E. Cabañas, and C. Arús, "The relationship between nuclear magnetic resonance-visible lipids, lipid droplets, and cell proliferation in cultured C6 cells," *Cancer Research*, vol. 59, no. 8, pp. 1861–1868, 1999.

[43] I. Barba, L. Chavarria, M. Ruiz-Meana, M. Mirabet, E. Agulló, and D. Garcia-Dorado, "Effect of intracellular lipid droplets on cytosolic Ca^{2+} and cell death during ischaemia-reperfusion injury in cardiomyocytes," *Journal of Physiology*, vol. 587, no. 6, pp. 1331–1341, 2009.

[44] P. L. Brasaemle, "A metabolic push to proliferate," *Science*, vol. 313, no. 5793, pp. 1581–1582, 2006.

[45] S. Uno, T. P. Dalton, P. R. Sinclair et al., "Cyp1a1(-/-) male mice: protection against high-dose TCDD-induced lethality and wasting syndrome, and resistance to intrahepatocyte lipid accumulation and uroporphyria," *Toxicology and Applied Pharmacology*, vol. 196, no. 3, pp. 410–421, 2004.

[46] N. Chauvet, T. El-Yandouzi, M. N. Mathieu et al., "Characterization of adherens junction protein expression and localization in pituitary cell networks," *Journal of Endocrinology*, vol. 202, no. 3, pp. 375–387, 2009.

[47] T. Soji, Y. Mabuchi, C. Kurono, and D. C. Herbert, "Folliculostellate cells and intercellular communication within the rat anterior pituitary gland," *Microscopy Research and Technique*, vol. 39, no. 2, pp. 138–149, 1997.

[48] M. Acosta, V. Filippa, and F. Mohamed, "Folliculo-stellate cells in pituitary pars distalis of male viscacha: immunohistochemical, morphometric and ultrastructural study," *European Journal of Histochemistry*, vol. 54, no. 1, pp. 1–9, 2010.